Energy Efficiency Optimization in Reconfigurable Intelligent Surface Aided Hybrid Multiuser mmWave MIMO Systems

JITENDRA SINGH [1] (Student Member, IEEE), **SURAJ SRIVASTAVA** [1] (Senior Member, IEEE),
SURYA P. YADAV [1] (Student Member, IEEE), **ADITYA K. JAGANNATHAM** [1] (Senior Member, IEEE),
AND LAJOS HANZO [2] (Life Fellow, IEEE)

[1]Electrical Engineering, Indian Institute of Technology Kanpur, Kanpur 208016, India
[2]Electronics and Computer Science, University of Southampton Highfield, SO17 1BJ Southampton, U.K.

CORRESPONDING AUTHOR: Lajos Hanzo (e-mail: lh@ecs.soton.ac.uk).

ABSTRACT   The energy efficiency (EE) of the reconfigurable intelligent surface (RIS) aided multiuser (MU) millimeterwave (mmWave) multi-input multi-output (MIMO) downlink is maximized by jointly optimizing the transmit power and number of active radio frequency (RF) chains. The base band (BB) transmit precoder (TPC) of this system is derived first by using the zero-forcing (ZF) technique for a given RF TPC and combiner at the base station (BS) as well as the phase shift matrix at the RIS. Furthermore, the ergodic sum-rate of the system is derived assuming a large number of antennas at the BS and users, followed by formulating the EE maximization problem subject to specific constraints imposed on the transmit power and on the number of RF chains. Then a low complexity sequential method is proposed for solving the above optimization problem, thus determining both the optimal transmit power and the number of active RF chains. Finally, simulation results are presented for demonstrating the improved EE performance of an RIS-aided mmWave MIMO system for a limited number of RF chains and transmit power at the BS.

INDEX TERMS   Energy efficiency, hybrid beamforming, millimeter wave, multiple-input multiple-output, reconfigurable intelligent surface.

I. INTRODUCTION

The millimeter wave (mmWave) band, which is comprised of frequencies in the range of 30–300 GHz, has attracted significant interest in the context of next-generation wireless systems as a benefit of having ample bandwidth [1]. However, communication in the mmWave band suffers from high pathloss and absorption losses [2]. The aforementioned challenges can be overcome by exploiting the numerous $\lambda/2$-spaced antenna elements within a compact space. The array gain can then be leveraged to compensate for the increased path-loss mentioned above. Hence, multi-input multi-output (MIMO) technology holds the key for the practical realization of mmWave communication. It must also be noted that the conventional fully-digital beamforming (FDB) architecture is not well suited for mmWave MIMO systems due to its high cost and increased power consumption, owing to requiring a separate radio frequency (RF) chain for each antenna element. To overcome this impediment, the pioneering works [3], [4], [5], [6], [7] proposed novel hybrid beamforming architectures that employ a significantly lower number of RF chains to design the hybrid beamformers (HBFs), which renders them cost- and energy-efficient. A significant problem in the high frequency mmWave band is that the transmit signal faces blockages, which prevent line of sight (LoS) communication. Reconfigurable intelligent surfaces (RIS) [8] can play an important role in overcoming this drawback by providing a few reflected communication paths for signal propagation. The authors of [9], [10], [11], [12], [13], [14] proposed

diverse RIS-enhanced wireless systems. Guo et al. [9], proposed an algorithm for jointly designing the active beamformer at the base station (BS) and passive beamformer at the RIS to maximize the weighted sum-rate of a downlink RIS-enabled multiuser (MU) multi-input single-output (MISO) wireless system. Yu et al. [10] optimize the RIS phase shift matrices in multi-RIS aided multi-cell systems to minimize the total time-frequency resource blocks subject to quality of service (QoS) constraint of the users. Ying et al. [11], extend the RIS-aided systems to mmWave MIMO technology, wherein they propose the geometric mean decomposition (GMD)-based joint active and passive beamformer to reduce the bit error rate of the system. Furthermore, Hong and Choi [12] uses the sparse scattering nature of mmWave MIMO systems to design a joint active HBF and passive beamformer for single user RIS-aided mmWave MIMO systems. As a further advance, Feng et al. [13] consider dynamically configured subarrays for jointly designing the active and passive HBFs based on successive interference cancellation. Li et al. [14] consider an RIS-aided MU mmWave MIMO system and minimize the transmit power at the BS by designing the HBF at the BS and passive beamformer at the RIS, subject to a QoS constraint for each user.

However, while RIS-aided wireless systems offer significant promise in terms of overcoming blockage and thereby improving the coverage, the data rates of these systems cannot be increased by simply boosting the transmit power, primarily due to environmental and cost concerns. Therefore, the improvement of energy efficiency (EE) of RIS-aided mmWave MIMO systems is one of the major goals of many researches in this area [15], [16]. Hence, You et al. [17] study the SE vs EE trade-off of RIS-aided MIMO uplink systems, where they jointly design the active TPC at each user and passive beamformer at the RIS to maximize the resource efficiency. Huang et al. [18] designed passive phase shifter at the RIS and optimized the power loading at the BS for maximizing the EE under the QoS constraint of each user of a downlink RIS-aided MU MISO system, while Du et al. [19] maximizes the EE of the RIS-aided multicast communication. Moreover, Ihsan et al. [20] jointly optimized the active beamforming at the BS, the passive beamforming at the IRS, and the power allocation at the users to maximize the EE of the RIS-aided non-orthogonal multiple access MIMO downlink. Furthermore, the authors of [21] have studied the trade off between spectral efficiency (SE) and EE in RIS-aided cognitive radio networks (CRNs) NOMA systems. As a further advance, the authors [22], [23] proposed innovative techniques based on the federated learning paradigm to optimize the EE of RIS-aided wireless networks. The authors of [24], [25], [26] optimized the transmit power and the number of active RF chains for maximizing the EE of mmWave MIMO systems, whereas Zheng et al. [25] proposed a low complexity energy efficient HBF. The authors of the pioneering work [26] proposed a framework for the joint optimization of the power and the number of active RF chains to maximize the EE of a mmWave MIMO system using spatial modulation.

Furthermore, Wang et al. [27] designed a novel lens antenna array at the BS for maximizing the EE in the multi-RIS assisted mmWave MISO downlink.

However, to best of our knowledge, none of the existing contributions have optimized the EE of an RIS-aided mmWave MU MIMO system with respect to both the transmit power and the number of active RF chains, which forms the focus of our work. Table 1 explicitly contrasts our novel contributions to the existing literature. The following are our main contributions:

- We commence by considering the model of the RIS-aided mmWave MU MIMO downlink with a limited number of active RF chains at the BS. Furthermore, we derive the ergodic sum-rate of the proposed system for a given HBF at the BS and phase shift matrix at the RIS.
- Then the EE maximization problem is formulated subject to constraints on both the transmit power and the number of RF chains. Then, a sequential method is conceived for the joint optimization of both the transmit power and the number of active RF chains together with the associated closed form solutions.
- Simulation results are presented to verify the accuracy of the theoretical closed-form solution and demonstrate the efficiency of proposed technique in enhancing the EE of RIS-aided mmWave MIMO systems.

In this article, we use boldface uppercase letters ($\mathbf{A}$) to denote matrices and boldface lowercase letters ($\mathbf{a}$) to represent vectors. The operator $(\cdot)^H$ denotes the Hermitian of a matrix; $|a|$ is the magnitude of a complex quantity a, while $\|\mathbf{a}\|^2$ represents the l_2 norm of a vector; $\mathbb{E}[\cdot]$ denotes the expectation operator; row($\mathbf{A}$) and col($\mathbf{A}$) denote the number rows and columns in a matrix $\mathbf{A}$; and $\mathbf{I}$ denotes an identity matrix.

II. RIS-AIDED MU MMWAVE MIMO SYSTEM AND CHANNEL MODELS
A. SYSTEM MODEL
We consider the RIS-aided MU mmWave downlink, where the BS having N_t transmit antennas and M_t RF chains is communicating with M users, each having N_r receive antennas and a single RF chain. An RIS with N reflective elements is assisting the communication between the BS and the users, as shown in Fig. 1. A hybrid transceiver architecture is used at the BS, which satisfies $M \leq M_t \leq N_t$, while analog beamforming is used at each SU. For achieving improved energy and cost efficiency, the minimum number of RF chains is used at the BS, i.e., $M_t = M$. Consider a data stream $\mathbf{s} = [s_1, \ldots, s_M]^T \in \mathbb{C}^{M \times 1}$, that has zero mean and a covariance matrix $\mathbf{I}_M$, which is first processed by the base band (BB) transmit precoder (TPC) $\mathbf{F}_{BB} \in \mathbb{C}^{M_t \times M}$, followed by the RF TPC $\mathbf{F}_{RF} \in \mathbb{C}^{N_t \times M_t}$. Consequently, the signal received at the mth user, denoted by $\mathbf{y}_m \in \mathbb{C}^{N_r \times 1}$, can be modeled as

$$\mathbf{y}_m = \sqrt{\rho}\mathbf{H}_m\mathbf{F}_{RF}\mathbf{F}_{BB}\mathbf{s} + \mathbf{n}_m$$
$$= \sqrt{\rho}\mathbf{H}_m\mathbf{F}_{RF}\mathbf{f}_{BB,m}s_m + \sum_{n=1,n\neq m}^{M}\sqrt{\rho}\mathbf{H}_m\mathbf{F}_{RF}\mathbf{f}_{BB,n}s_n + \mathbf{n}_m, \quad (1)$$

TABLE 1. Summary of Literature Survey on EE Optimization in RIS-Aided mmWave MIMO Systems

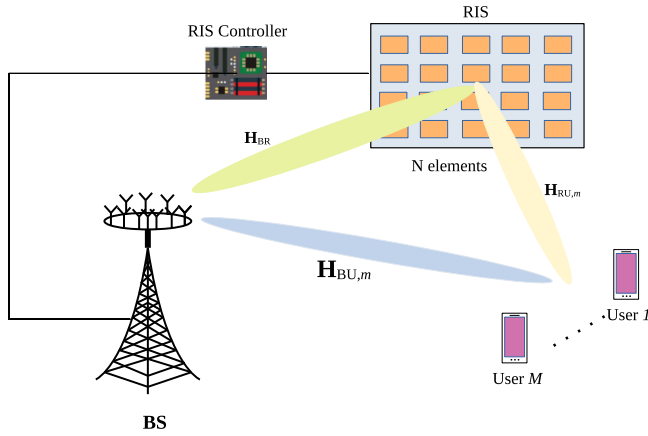|	[11]	[12]	[14]	[18]	[19]	[20]	[23]	[24]	[25]	[27]	Our
mmWave MIMO	✓	✓	✓					✓	✓	✓	✓
RIS	✓	✓	✓	✓	✓	✓	✓			✓	✓
Multiple users			✓	✓	✓	✓	✓	✓			✓
EE				✓	✓	✓	✓	✓	✓	✓	✓
Closed-form solution		✓					✓		✓		✓
Optimal transmit power		✓	✓	✓	✓		✓				✓
Adaptive number of active RF chains								✓	✓		✓
Low-complexity joint optimization			✓								✓

FIGURE 1. RIS-aided MU mmWave MIMO downlink system.

where $\rho = \frac{P}{M}$ is the equal power allocation of each user, where P denotes the total transmit power of the BS, $\mathbf{f}_{\text{BB},m} \in \mathbb{C}^{M_t \times 1}$ is the BB TPC of the mth user and $\mathbf{n}_m \in \mathbb{C}^{N_r \times 1}$ denotes the circularly symmetric additive white Gaussian noise (AWGN) distributed as $\mathcal{CN}(\mathbf{0}, \sigma^2 \mathbf{I})$. Furthermore, $\mathbf{H}_m = \mathbf{H}_{\text{BU},m} + \mathbf{H}_{\text{RU},m} \mathbf{\Phi} \mathbf{H}_{\text{BR}} \in \mathbb{C}^{N_r \times N_t}$ represents the block-fading mmWave MIMO channel between the BS and the mth user, where $\mathbf{H}_{\text{BU},m} \in \mathbb{C}^{N_r \times N_t}$ is the channel spanning from the BS to the mth user, while $\mathbf{H}_{\text{BR}} \in \mathbb{C}^{N \times N_t}$ and $\mathbf{H}_{\text{RU},m} \in \mathbb{C}^{N_r \times N}$ represent the BS to the RIS link and RIS to the mth user link, respectively. The variable $\mathbf{\Phi} \in \mathbb{C}^{N \times N}$ represents the phase shift matrix of the RIS. Assuming that each reflective unit of the RIS reflects the incident signal independently, $\mathbf{\Phi}$ can be modelled as $\mathbf{\Phi} = \text{diag}([e^{j\theta_1}, \dots, e^{j\theta_N}]) \in \mathbb{C}^{N \times N}$ [14]. Furthermore, the BS can acquire the global CSI of all the links via uplink channel estimation, in which each user transmits its pilot symbols to the BS within different time slots, allowing the BS to estimate each cascaded and direct CSI [28], [29], [30], [31], [32]. The receive signal $\bar{y}_m$ after processing by the combiner $\mathbf{w}_m$ at the mth user is given by

$$\bar{y}_m = \mathbf{w}_m^H \mathbf{y}_m$$
$$= \sqrt{\rho} \mathbf{w}_m^H \mathbf{H}_m \mathbf{F}_{\text{RF}} \mathbf{f}_{\text{BB},m} s_m$$
$$+ \sum_{n=1, n \neq m}^{M} \sqrt{\rho} \mathbf{w}_m^H \mathbf{H}_m \mathbf{F}_{\text{RF}} \mathbf{f}_{\text{BB},n} s_n + \bar{n}_m, \quad (2)$$

where $\mathbf{w}_m \in \mathbb{C}^{N_r \times 1}$ is the RF combiner and $\bar{n}_m = \mathbf{w}_m^H \mathbf{n}_m$ is the combined noise at the mth user. One can use the procedure described in [6] to design the RF TPC $\mathbf{F}_{\text{RF}}$ and the combiner $\mathbf{w}_m, \forall m$, where $\mathbf{F}_{\text{RF}}^H \mathbf{F}_{\text{RF}} = \mathbf{I}_{M_t}$ and $\mathbf{w}_m^H \mathbf{w}_m = 1$. Using (2), and assuming Gaussian transmitted symbols over a mmWave channel, the rate of user m is given by

$$\mathcal{R}_m = \log_2 (1 + \gamma_m), \quad (3)$$

where γ_m is the resultant signal to interference plus noise power ratio (SINR) of user m, which is given by

$$\gamma_m = \frac{\rho \left| \mathbf{w}_m^H \mathbf{H}_m \mathbf{F}_{\text{RF}} \mathbf{f}_{\text{BB},m} \right|^2}{\rho \sum_{n=1, n \neq m}^{M} \left| \mathbf{w}_m^H \mathbf{H}_m \mathbf{F}_{\text{RF}} \mathbf{f}_{\text{BB},n} \right|^2 + \sigma^2 \|\mathbf{w}_m\|_2^2}. \quad (4)$$

B. MMWAVE MIMO CHANNEL

The Saleh-Valenzuela model can be invoked to represent the mmWave MIMO channel [6], [12], as

$$\mathbf{H}_i = \sum_{l=1}^{N_i^p} \alpha_{i,l} \mathbf{a}_r \left(\phi_{i,l}^r, \theta_{i,l}^r \right) \mathbf{a}_t^H \left(\phi_{i,l}^t, \theta_{i,l}^t \right), \quad (5)$$

where the subscript $i \in \{\{\text{BU}, m\}, \text{BR}, \{\text{RU}, m\}\}$ represents the corresponding link, N_i^p denotes the number of multipath components and $\alpha_{i,l}$ is the complex gain of the lth multipath component. The quantity $\alpha_{i,l} \sim \mathcal{CN}(0, \gamma_i^2 10^{-0.1 PL(d_i)}), \forall l$, where $\gamma_i = \sqrt{\text{row}(\mathbf{H}_i)\text{col}(\mathbf{H}_i)/N_i^p}$ is a normalization factor and $PL(d_i)$ represents the path loss with d_i denoting the length of the link. Furthermore, $\mathbf{a}_t(\phi_{i,l}^t \theta_{i,l}^t) \in \mathbb{C}^{\text{col}(\mathbf{H}_i) \times 1}$ and $\mathbf{a}_r(\phi_{i,l}^r \theta_{i,l}^r) \in \mathbb{C}^{\text{row}(\mathbf{H}_i) \times 1}$ represent the transmit and receive array response vectors, where $\phi_{i,l}^t(\theta_{i,l}^t)$ and $\phi_{i,l}^r(\theta_{i,l}^r)$ are the azimuth (elevation) angles of departures (AoDs) and arrivals (AoAs), respectively. For the uniform planar arrays (UPAs) employed at the BS, RIS, and each user, the array response vectors can be written as

$$\mathbf{a}_z (\phi, \theta) = \frac{1}{\sqrt{N_z}} \Big[1, \dots, e^{j \frac{2\pi}{\lambda} d(o \sin \phi \sin \theta + p \cos \theta)}$$
$$\dots, e^{j \frac{2\pi}{\lambda} d((N_z^h - 1) \sin \phi \sin \theta + (N_z^v - 1) \cos \theta)} \Big]^T, \quad (6)$$

where $z \in \{\text{r}, \text{t}\}$ and $0 \leq o < N_z^h$, and $0 \leq p < N_z^v$ are the indices of the horizontal and vertical antennas or RIS elements, respectively. Furthermore, λ is the wavelength, and d is the

spacing between the antennas or the RIS elements, where the latter is spaced at half the wavelength.

III. ENERGY EFFICIENCY MODELING

In the procedure described in this section, the HBF and RIS phase shifters are assumed to be designed alternatively, i.e. the HBFs $\mathbf{F}_{RF}$, $\mathbf{F}_{BB}$ and $\mathbf{w}_m$, $\forall m$, are designed for a fixed phase shifter matrix $\boldsymbol{\Phi}$, and vice versa. Let us assume that the analog beamformers $\mathbf{F}_{RF}$, $\mathbf{w}_m$, $\forall m$, are designed using the low-complexity TPC method of [6]. Therefore, the effective channel $\overline{\mathbf{H}} \in \mathbb{C}^{M \times M_t}$ after RF TPC and combining is given by

$$\overline{\mathbf{H}} = \left[\overline{\mathbf{h}}_1, \ldots, \overline{\mathbf{h}}_M\right]^H, \tag{7}$$

where $\overline{\mathbf{h}}_m^H = \mathbf{w}_m^H \mathbf{H}_m \mathbf{F}_{RF} \in \mathbb{C}^{1 \times M_t}$. Additionally, the BB TPC $\widetilde{\mathbf{F}}_{BB}$ is designed using the ZF TPC, which is given by

$$\widetilde{\mathbf{F}}_{BB} = \overline{\mathbf{H}}\left(\overline{\mathbf{H}}^H \overline{\mathbf{H}}\right)^{-1}. \tag{8}$$

Therefore, the normalized BB TPC considering the power constraint is given by

$$\mathbf{F}_{BB} = \frac{\sqrt{P}\widetilde{\mathbf{F}}_{BB}}{\mathbf{F}_{RF}\widetilde{\mathbf{F}}_{BB}}. \tag{9}$$

Based on the above HBF design, the resultant MUI-free signal $\widetilde{y}_m$ at the mth user can be written as

$$\widetilde{y}_m = \sqrt{\rho}\mathbf{w}_m^H \mathbf{H}_m \mathbf{F}_{RF}\mathbf{f}_{BB,m}s_m + \overline{n}_m. \tag{10}$$

Furthermore, for a fixed TPC $\mathbf{F}_{RF}\mathbf{F}_{BB}$ and combiner $\mathbf{w}_m$, $\forall m$, the RIS phase shift matrix $\boldsymbol{\Phi}$ can be designed using one of the methods available in the literature [12], [13], [14].

By exploiting the fact that all the users collaborate with each other to cancel the MUI, the mutual information $\mathcal{I}_m$ of the mth user obeying (10) is given by

$$\mathcal{I}_m = \log_2\left(1 + \frac{P}{M\sigma^2}a_m\right), \tag{11}$$

where $a_m = |\overline{\mathbf{h}}_m^H \mathbf{f}_{BB,m}|^2$ is the beamforming gain. Furthermore, the achievable rate of the mth user for discrete symbol inputs can be upper bounded as

$$\mathcal{R}_m \leq \mathcal{I}_m. \tag{12}$$

Upon assuming that $\overline{\mathbf{h}}_m$, $\forall m$, are identically distributed due to the fact that each user is facing identically fading channels, the ergodic sum-rate of the system can be formulated as

$$\begin{aligned}
\mathcal{R}_{sum} &= \sum_{m=1}^{M}\mathbb{E}[\mathcal{R}_m] \\
&= M\mathbb{E}[\mathcal{R}_m] \\
&= M\mathbb{E}_{a_m}\left[\log_2\left(1 + \frac{P}{M\sigma^2}a_m\right)\right], \tag{13}
\end{aligned}$$

where $\mathbb{E}_{a_m}[\cdot]$ is the expectation with respect to the random variable a_m. Using the Jensen's inequality, one can upper-bound the quantity $\mathcal{R}_{sum}$ as

$$\mathcal{R}_{sum} \leq M\log_2\left(1 + \frac{P}{M\sigma^2}\mathbb{E}_{a_m}[a_m]\right). \tag{14}$$

At this juncture, employing the large antenna array approximation for the ZF BB TPC and unit magnitude constraints on the elements of $\mathbf{F}_{RF}$, the quantity $\mathbb{E}_{a_m}[a_m]$ can be written as

$$\mathbb{E}_{a_m}[a_m] = \|\mathbf{f}_{BB,m}\|^2 b_m, \tag{15}$$

where $b_m = \mathbf{w}_m^H \mathbb{E}[\mathbf{H}_m \mathbf{H}_m^H]\mathbf{w}_m$. As shown in Appendix A, the quantity b_m can be simplified to

$$b_m = N_t N_r\left[2 \times 10^{-0.1PL(d_i)} + \frac{N^2}{N^p} \times 10^{-0.2 \times PL(d_i)}\right]. \tag{16}$$

Furthermore, the power dissipation P_{diss} for the given downlink system can be modeled as [17], [25]

$$P_{diss} = \eta P + MP_c, \tag{17}$$

where $\eta > 0$ is the amplifier efficiency, while P_c represents the hardware power required for each user. Additionally, P_c is calculated as $P_c = P_{BS} + P_{RIS}$, where P_{BS} is the static power consumed at the BS and $P_{RIS} = NP_n(b)$ is the power consumption of the RIS. Here, $P_n(b)$ represents the power required for each phase shifter having b bits of resolution, where the typical values of $P_n(b)$ are 1.5, 4.5, 6, and 7.8 mW for $3-$, $4-$, $5-$, and $6-$bit resolution phase shifters [18]. Using (13) and (17), the EE of the system in bits/Hz/J, which is defined as ratio of the achievable sum-rate to the power consumption, can be expressed as

$$EE(P, M) = \frac{M\log_2\left(1 + \frac{P}{M}c_m\right)}{\eta P + MP_c}, \tag{18}$$

where $c_m = \frac{\|\mathbf{f}_{BB,m}\|^2 b_m}{\sigma^2}$. As a result, the optimization problem to maximize the EE of the system with respect to the transmit power P and number of users M, can be formulated as

$$\begin{aligned}
\left(P^{opt}, M^{opt}\right) &= \arg\max_{P,M} EE(P, M) \\
\text{s.t. } & 0 \leq P \leq P_{max}, \\
& M = \{1, \ldots M_{max}\}, \tag{19}
\end{aligned}$$

where P_{max} is the maximum allowable transmit power at the BS, and M_{max} denotes the feasible value of the maximum number of active RF chains/users. The above design problem is challenging to solve with respect to the variables P and M due to the fact that M is constrained to take only integer values, which renders it a non-convex problem. Our novel approach to solve the above problem is described next.

IV. ENERGY EFFICIENT RESOURCE ALLOCATION

In order to solve (19), we begin by defining the variable $z = \frac{P}{M}$, which transforms the integer variable M of the objective function to the continuous variable z that is positive real valued. As a result, the EE of the system is a function of the

single variable z. Hence, the modified optimization problem can be recast as

$$z^{\text{opt}} = \arg\max_z \frac{\left[\log_2\left(1+zc_m\right)\right]}{\eta z + P_c}$$

$$\text{s.t. } 0 \leq z \leq \frac{P_{max}}{M},$$

$$M = \{1, \ldots M_{\max}\}. \tag{20}$$

To solve the above optimization problem, let us consider the unconstrained optimization function $f(z) = \frac{\log_2\left(1+zc_m\right)}{\eta z + P_c}$, which is a quasiconcave function with respect to the variable z, since the set $S_\alpha = \{z : f(z) \geq \alpha\} = \{z : \alpha(\eta z + P_c) - \log_2\left(1+zc_m\right) \leq 0\}$ is strictly convex for $\alpha \in \mathbb{R}$. Therefore, there exists a global maximum z^{opt} at $f'(z) = 0$, and the function $f(z)$ initially increases for $0 \leq z \leq z^{\text{opt}}$ and decreases subsequently for $z > z^{\text{opt}}$. We now determine z^{opt} by setting

$$f'(z) = 0 \Rightarrow \frac{c_m(P_c + \eta z)}{(1+zc_m)\log_e(2)} - \log_2(1+zc_m)\eta = 0. \tag{21}$$

The above equation can be further simplified as

$$\frac{c_m(P_c + \eta z)}{(1+zc_m)} = \eta \log_e(1+zc_m). \tag{22}$$

Then equation (22) can be further reduced as

$$\frac{c_m P_c - \eta}{(1+zc_m)} = \eta[\log_e(1+zc_m) - 1] \Rightarrow z = \frac{e^{x+1}-1}{c_m}, \tag{23}$$

where $x = \log_e(1+zc_m) - 1$. Substituting $(1+zc_m) = e^{x+1}$ in the above equation results in

$$\frac{c_m P_c - \eta}{\eta e} = xe^x. \tag{24}$$

Therefore, the unconstrained solution of (20) is given by

$$z^{\text{opt}} = \frac{e^{W\left(\frac{c_m P_c - \eta}{\eta e}\right)+1} - 1}{c_m}, \tag{25}$$

where $W(x)$ is the Lambert W function, which is defined as $x = W(x)e^{W(x)}$, for $x \in \mathbb{C}$ [33].

In order to find the solution of the constrained problem (20), two cases can be considered as described below.

i) $z^{\text{opt}} \leq P_{\max}$: In this case, the point z^{opt} is feasible for (20), which results in the optimal pair of the form $(M, P = z^{\text{opt}}M)$. Note that the largest M to satisfy $P \leq P_{\max}$ is given by

$$\overline{M} = \left\lfloor \frac{P_{max}c_m}{e^{W\left(\frac{c_m P_c - \eta}{\eta e}\right)+1} - 1} \right\rfloor. \tag{26}$$

Furthermore, upon taking the last constraint of (19) into account, the optimal number of users is formulated as

$$M^{\text{opt}} = \min\left(\overline{M}, M_{\max}\right). \tag{27}$$

Step 0. Main objective:

Maximizing the energy efficiency (EE) shown in (18)

Step 1. Active HBF:

Compute HBFs F_{RF}, F_{BB} and w_m for the fixed RIS phase shifter matrix Φ as discussed in Section III.

Step 2. Passive beamforming:

Evaluate the RIS phase shift matrix Φ using (34) for the fixed active beamformers F_{RF}, F_{BB} and w_m.

Step 3. Optimization problem:

Finding the optimal transmit power P and the number of active RF chains (users) M, which maximizes EE as shown in (19).

Step 4. Joint optimization to solve (19):

Solving the optimization problem (19) is challenging with respect to the variables P and M because M is constrained to take only integer value, which renders it a non-convex problem.

Step 5. Adopted strategy to solve (19):

To solve (19), a sequential method is adopted to jointly optimize both P and M with the associated closed-form solutions, as given by (27) and (28).

FIGURE 2. Flow of the proposed mathematical analysis.

As a result, the optimal power for these M^{opt} number of users is obtained as

$$P^{\text{opt}} = z^{\text{opt}} M^{\text{opt}}. \tag{28}$$

ii) $z^{\text{opt}} > P_{\max}$: This scenario results in $z^{\text{opt}} > \frac{P_{\max}}{M}$, which is infeasible due to the maximum transmit power constraint at the BS.

Furthermore, the flow of the mathematical analysis of the proposed scheme for maximizing the EE of the considered system is shown in Fig. 2.

V. COMPLEXITY ANALYSIS OF THE PROPOSED DESIGN

In this section we analyze the computational complexity of the proposed energy efficient resource allocation method. Observe that the complexity of the RIS phase shift design based on (34) is given by $\mathcal{O}(N_t N_r N)$. Moreover, the optimal number of users and power are computed using the closed-form expressions given by (27) and (28), respectively. Note that both expressions (27) and (28) are independent of the instantaneous CSI. Explicitly, they only depend on the channel statistics, which results in low complexity as compared to the design of the RIS phase shift matrix. As a result, the overall complexity of the proposed method is dominated by $\mathcal{O}(N_t N_r N)$.

VI. SIMULATION RESULTS

This section presents on simulation results to quantifies the EE of the system for the proposed scheme. Our simulation setup is comprised of a BS located at the origin $(0,0)$ in a 2-D region, while the RIS is placed at the coordinates $(d_{\text{RIS}}, 50)\text{m}$,
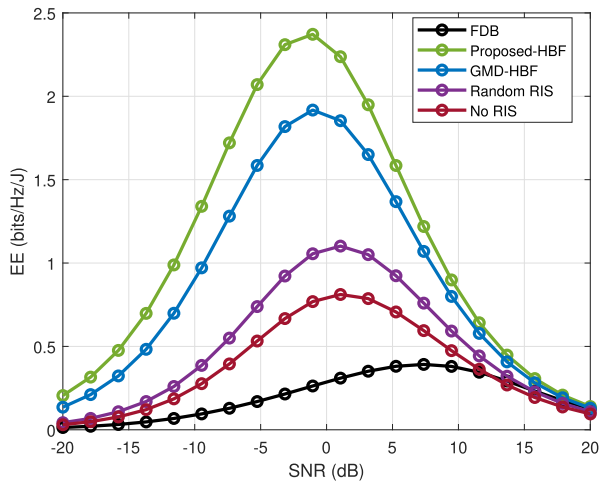
FIGURE 3. EE versus SNR of an 8×128 RIS-aided MU mmWave MIMO system with $N = 128$.

FIGURE 4. EE versus N_t of an RIS-aided MU mmWave MIMO system with $N = 128$.

where d_{RIS} is the horizontal distance of the RIS from the BS. The users are placed randomly obeying a uniform distribution within a circle of 10m radius that is centred at $(100, 0)$m. The BS is assumed to have $N_t = 128$ transmit antennas and $M_t = M$ RF chains, whereas the number of users M is set to 4, with each possessing $N_r = 8$ receiving antennas together with a single RF chain. The number of RIS elements N is set to 128. The mmWave MIMO channels are generated using (5) and the pathloss model is given as [12]
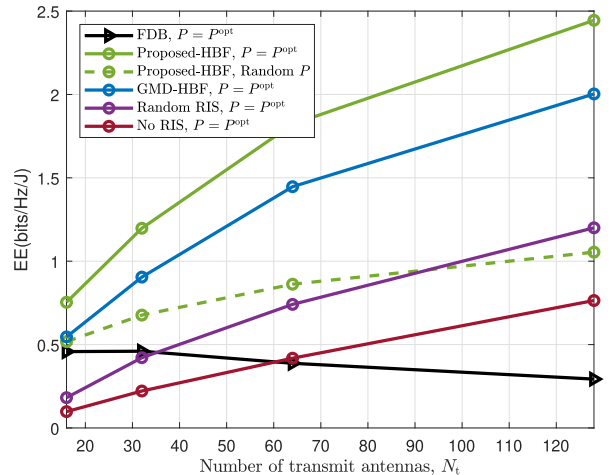
$$PL(d_i) \, [\mathrm{dB}] = \beta_1 + \beta_2 10 \log_{10}(d_i) + \xi, \qquad (29)$$

where $\beta_1 = 61.4$, $\beta_2 = 2$ and $\xi \sim \mathcal{N}(0, \sigma_\zeta^2)$ with $\sigma_\zeta = 5.8$ dB for LoS paths and $\beta_1 = 72.0$, $\beta_2 = 2.92$ and $\sigma_\zeta = 8.7$ dB for non-LoS paths according to the experimental data for the 28 GHz band. Furthermore, the discrete phase shifters at the RIS are configured from the set

$$\mathcal{S} = \left\{ e^{j\theta} \Big| \theta \in \left\{ 0, \frac{2\pi}{2^b}, \dots, \frac{2\pi(2^b - 1)}{2^b} \right\} \right\}, \qquad (30)$$

where we assume $b = 3$ bits for the quantization of the phase shift values. Furthermore, the static hardware power P_{BS}, amplifier efficiency η and noise power σ^2 are assumed to be 30 dBm, 0.3 and -91 dBm, respectively. We fix the distance d_{RIS} between the BS and RIS to be 50 m and define the SNR as $\frac{P}{M\sigma^2}$.

In Fig. 3, we plot the EE versus SNR for the proposed scheme and compare the results to that of the FDB, GMD-based design [11], Random RIS design and no RIS. For Random RIS design, the phases of the each RIS element are selected randomly from $[0, 2\pi)$, while for No RIS design, the RIS is absent in the system model. Observe from the figure that the EE initially increases upon increasing the SNR and achieves its maximum at P^{opt}. Subsequently, it decreases for a further increase of the SNR. Furthermore, the EE of the proposed-HBF is better than that of the GMD-HBF, which is due to the fact that the GMD-HBF scheme aims to minimize the BER instead of maximizing the rate. Additionally, the

proposed design outperforms the Random RIS and No RIS scheme, which shows the importance of the judicious design of the RIS phase shift matrix. Note that the FDB has the worst EE due to the requirement of a large number of power hungry RF chains.

Fig. 4 depicts the EE versus number of transmit antennas N_t at the BS for the optimal transmit power P^{opt} and a randomly chosen value $P < P_{\max}$. It can be observed that the EE of the proposed scheme increases almost linearly upon increasing N_t as it leads to a linear increment of P^{opt}, which eventually results in a corresponding increase in the EE. This is due to the fact that there is a linear increment in the quantity $\frac{e^{W(\frac{c_m P_c - \eta}{\eta e}) + 1} - 1}{c_m}$ for large values of c_m, whereas c_m is proportional to N_t, as seen from (16). Moreover, it can also be observed from Fig. 4 that the EE for an arbitrary value of the power P lags behind the EE for the optimal value P^{opt}, which corroborates the efficiency of our proposed scheme. Furthermore, the EE of the FDB decreases after $N_t = 30$ due to the requirement of $M_t = N_t$. On the other hand, the EE of the GMD-HBF, Random RIS and No RIS designs increase linearly with N_t for $P = P^{\mathrm{opt}}$, but it remains inferior to the EE of the proposed-HBF design. This demonstrates the efficacy of our proposed design in terms of the EE of the RIS-aided systems.

Fig. 5 shows the EE of the system versus the number of users M, who are assumed to be distributed uniformly in the circle of radius 10 m. A fixed power of $P = P^{\mathrm{opt}}$ is used for all the schemes in this analysis. Observe that as M increases, the EE decreases, which is due to the increased MUI and the reduced transmit power per user. Additionally, the proposed-HBF design performs better than the other schemes, which justifies the importance of the proposed RIS phase shift matrix design in terms of maximizing the EE of MU communication.

In Fig. 6, we plot the EE versus N of an 8×128 system with $M = 4$ and $P = P^{\mathrm{opt}}$, $P_n(b) = 1.5$ mW and $P_n(b) = 7.8$ mW. It can be observed that the EE increases with N for $N <$
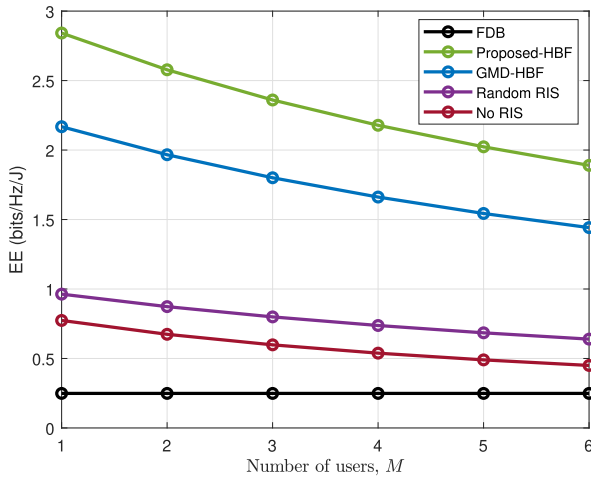
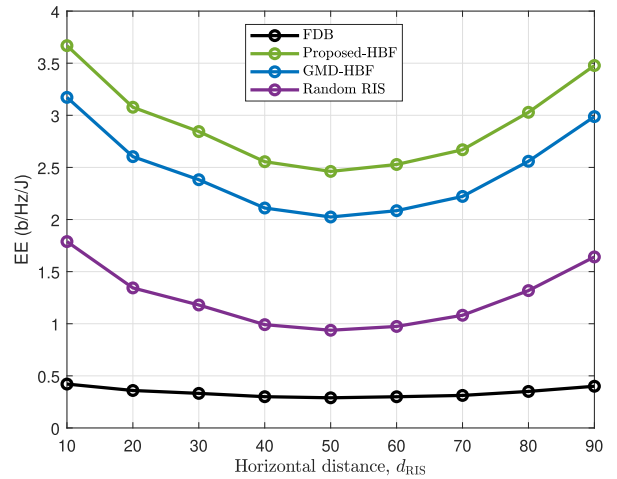**FIGURE 5.** EE versus *M* of an 8 × 128 RIS-aided MU mmWave MIMO system with *N* = 128.

FIGURE 6. EE versus *N* of an 8 × 128 RIS-aided MU mmWave MIMO system.

FIGURE 7. EE versus d_{RIS} of an 8 × 128 RIS-aided MU mmWave MIMO system with *N* = 128.

FIGURE 8. EE versus SNR of a RIS-aided MU mmWave MIMO system for different number of transmit antennas.

400 at $P_n(b) = 1.5$mW and then it starts decreasing for $N >$ 400. However, this trend happens at $N = 200$ for $P_n(b) = 7.8$ mW for all the schemes. This shows that for a given $P_n(b)$ and P, there is an optimal value of the number of RIS elements N for which the EE is maximum. Hence, a large N may increase the sum-rate of the system, but at the cost of reducing the EE of the system. Also, the proposed-HBF design outperforms all the other benchmarks at each value of N for both $P_n(b) = 1.5$ mW and $P_n(b) = 7.8$ mW, which demonstrates that the design can be beneficially employed in practical RIS-aided mmWave MIMO systems.

In Fig. 7, we investigate the EE of the system with respect to the horizontal distance d_{RIS} of the RIS from the BS. It can be observed from the figure that the EE of all the schemes initially decrease upon increasing the distance and achieve their minimum at $d_{RIS} = 50$m. Then subsequently further both increase with distance. Therefore, it is beneficial to place the RIS near the BS or closer to the users for improving the EE.
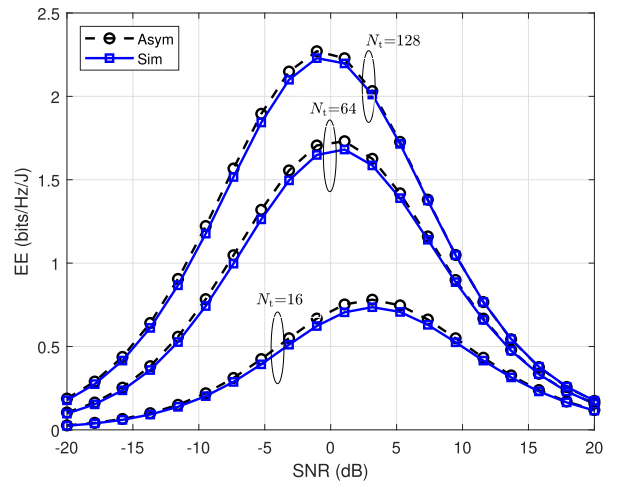
Finally in Fig. 8, we plot the asymptotic EE (labeled as Asym) and simulated EE (labeled as Sim) vs SNR for different values of the number of transmit antennas N_t for $N = 128$ RIS elements. As seen from the figure, the simulated EE approaches the asymptotic EE as N_t increases from 16 to 128, which validates the asymptotic analysis presented in Section III. Additionally, it can be observed from this figure that the asymptotic EE in (18) can be regarded as an upper bound of the achievable EE of the system.

VII. SUMMARY AND CONCLUSION

We conceived a technique for the joint optimization of the transmit power and the number of active RF chains (users) for the RIS-aided mmWave MU MIMO downlink. For a given HBF at the BS, and phase shift matrix at the RIS, the optimization problem is formulated for EE maximization under the constraints of a given total transmit power and number of RF chains. Subsequently, the global maximum of the above problem is determined and closed form solutions are presented for

the optimal power and number of active RF chains (users) in the system. Our simulation results show the efficiency of the proposed scheme in improving the EE of RIS-aided systems.

$$= N_\text{t} N_\text{r} \left[2 \times 10^{-0.1 PL(d_i)} + \frac{N^2}{N^\text{p}} \times 10^{-0.2 \times PL(d_i)} \right]. \quad (37)$$

APPENDIX A
DERIVATION FOR (16)

The quantity $\mathbb{E}[\mathbf{H}_m \mathbf{H}_m^H]$ can be evaluated as

$$\mathbb{E}\left[\mathbf{H}_m \mathbf{H}_m^H \right]$$
$$= \mathbb{E}\left[(\mathbf{H}_{\text{BU},m} + \mathbf{H}_{\text{RU},m} \mathbf{\Phi} \mathbf{H}_{\text{BR}})(\mathbf{H}_{\text{BU},m} + \mathbf{H}_{\text{RU},m} \mathbf{\Phi} \mathbf{H}_{\text{BR}})^H \right]$$
$$= \mathbb{E}\left[\mathbf{H}_{\text{BU},m} \mathbf{H}_{\text{BU},m}^H + \mathbf{H}_{\text{BU},m} \mathbf{H}_{\text{BR}}^H \mathbf{\Phi}^H \mathbf{H}_{\text{RU},m}^H \right.$$
$$\left. + \mathbf{H}_{\text{RU},m} \mathbf{\Phi} \mathbf{H}_{\text{BR}} \mathbf{H}_{\text{BU},m}^H + \mathbf{H}_{\text{RU},m} \mathbf{\Phi} \mathbf{H}_{\text{BR}} \mathbf{H}_{\text{BR}}^H \mathbf{\Phi}^H \mathbf{H}_{\text{RU},m}^H \right]. \quad (31)$$

Upon invoking the asymptotic orthogonality property, i.e., as $N_\text{t} \to \infty$ [12], we have

$$\mathbf{a}_\text{t}^H \left(\phi_{\text{BU},m,l}^\text{t} \right) \mathbf{a}_\text{t} \left(\phi_{\text{BR},l}^\text{t} \right) \to 0, \quad (32)$$

for $\phi_{\text{BU},m,l}^\text{t} \neq \phi_{\text{BR},l}^\text{t}$. Using the above argument, (31) simplifies to

$$\mathbb{E}\left[\mathbf{H}_m \mathbf{H}_m^H \right]$$
$$= \mathbb{E}\left[\mathbf{H}_{\text{BU},m} \mathbf{H}_{\text{BU},m}^H + \mathbf{H}_{\text{RU},m} \mathbf{\Phi} \mathbf{H}_{\text{BR}} \mathbf{H}_{\text{BR}}^H \mathbf{\Phi}^H \mathbf{H}_{\text{RU},m}^H \right]. \quad (33)$$

According to Proposition 2 in [12], the optimal RIS phase shift matrix for the given system is

$$\mathbf{\Phi}^* = N \mathcal{D} \left(\mathcal{D} \left(\mathbf{a}_\text{r} \left(\phi_{\text{BR},l^*}^\text{r}, \theta_{\text{BR},l^*}^\text{r} \right) \right) \mathbf{a}_\text{t} \left(\phi_{\text{RU},m,l^*}^\text{t}, \theta_{\text{RU},m,l^*}^\text{t} \right) \right), \quad (34)$$

where $\mathcal{D}(\mathbf{x})$ denotes the diagonal matrix that contains vector $\mathbf{x}$ on its main diagonal and l^* is the best path for the worst-case user. Using the above design of $\mathbf{\Phi}^*$ and $N_i^\text{p} = N^\text{p}, \forall i$, one can rewrite (33) as

$$\mathbb{E}\left[\mathbf{H}_m \mathbf{H}_m^H \right] = \mathbb{E}\left[\sum_{l=1}^{N^\text{p}} |\alpha_{\text{BU},m,l}|^2 \, \mathbf{a}_\text{r} \left(\phi_{\text{BU},m,l}^\text{r}, \theta_{\text{BU},m,l}^\text{r} \right) \right.$$
$$\mathbf{a}_\text{r}^H \left(\phi_{\text{BU},m,l}^\text{r}, \theta_{\text{BU},m,l}^\text{r} \right) + |\alpha_{\text{RU},m,l^*}|^2 \, |\alpha_{\text{BR},l^*}|^2$$
$$\left. \times \mathbf{a}_\text{r} \left(\phi_{\text{RU},m,l^*}^\text{r}, \theta_{\text{RU},m,l^*}^\text{r} \right) \mathbf{a}_\text{r}^H \left(\phi_{\text{RU},m,l^*}^\text{r}, \theta_{\text{RU},m,l^*}^\text{r} \right) \right]. \quad (35)$$

In the large antenna regime, $\mathbf{a}_\text{r}(\phi_{i,l}^\text{r}, \theta_{i,l}^\text{r}) \mathbf{a}_\text{r}^H(\phi_{i,l}^\text{r}, \theta_{i,l}^\text{r}) \to \mathbf{I}_{N_\text{r}}, \forall i, l$ [3]. Therefore, (35) can be simplified as

$$\mathbb{E}\left[\mathbf{H}_m \mathbf{H}_m^H \right] = \mathbb{E}\left[\sum_{l=1}^{N^\text{p}} |\alpha_{\text{BU},m,l}|^2 + |\alpha_{\text{RU},m,l^*}|^2 \, |\alpha_{\text{BR},l^*}|^2 \right] \mathbf{I}_{N_\text{r}}. \quad (36)$$

Furthermore, from $\alpha_{i,l} \sim \mathcal{CN}(0, \gamma_i^2 10^{-0.1 PL(d_i)})$, we have $\sum_{l=1}^{N^\text{p}} |\alpha_{i,l}|^2 \sim \Gamma(N^\text{p}, 2\gamma_i^2 10^{-0.1 PL(d_i)})$ and $|\alpha_{i,l}|^2 \sim \exp(\frac{1}{\gamma_i^2 10^{-0.1 PL(d_i)}})$, where $\Gamma(\cdot)$ and $\exp(\cdot)$ denote the Gamma and exponential distributions, respectively. Therefore, b_m is given by

$$b_m = \mathbf{w}_m^H \mathbb{E}\left[\mathbf{H}_m \mathbf{H}_m^H \right] \mathbf{w}_m$$

REFERENCES

[1] T. S. Rappaport et al., "Millimeter wave mobile communications for 5G cellular: It will work!," *IEEE Access*, vol. 1, pp. 335–349, 2013.

[2] R. W. Heath, N. González-Prelcic, S. Rangan, W. Roh, and A. M. Sayeed, "An overview of signal processing techniques for millimeter wave MIMO systems," *IEEE J. Sel. Topics Signal Process.*, vol. 10, no. 3, pp. 436–453, Apr. 2016.

[3] O. E. Ayach, S. Rajagopal, S. Abu-Surra, Z. Pi, and R. W. Heath, "Spatially sparse precoding in millimeter wave MIMO systems," *IEEE Trans. Wireless Commun.*, vol. 13, no. 3, pp. 1499–1513, Mar. 2014.

[4] K. Satyanarayana, M. El-Hajjar, P.-H. Kuo, A. Mourad, and L. Hanzo, "Hybrid beamforming design for full-duplex millimeter wave communication," *IEEE Trans. Veh. Technol.*, vol. 68, no. 2, pp. 1394–1404, Feb. 2019.

[5] A. A. Nasir, H. D. Tuan, T. Q. Duong, H. V. Poor, and L. Hanzo, "Hybrid beamforming for multi-user millimeter-wave networks," *IEEE Trans. Veh. Technol.*, vol. 69, no. 3, pp. 2943–2956, Mar. 2020.

[6] J. Singh, I. Chatterjee, S. Srivastava, A. Agrahari, A. K. Jagannatham, and L. Hanzo, "Hybrid transceiver design and optimal power allocation for the cognitive mmWave multiuser MIMO downlink relying on limited feedback," *IEEE Open J. Veh. Technol.*, vol. 4, pp. 241–256, 2023.

[7] J. Singh, I. Chatterjee, S. Srivastava, and A. K. Jagannatham, "Hybrid transceiver design and optimal power allocation in downlink mmWave hybrid MIMO cognitive radio systems," in *Proc. IEEE Nat. Conf. Commun.*, 2022, pp. 178–183.

[8] J.-B. Wang, X. Wang, F. Yang, H. Zhang, M. Lin, and J. Wang, "Intelligent reflecting surface aided millimeter wave communication using subarray-connected structure," *IEEE Trans. Veh. Technol.*, vol. 71, no. 5, pp. 5581–5586, May 2022.

[9] H. Guo, Y.-C. Liang, J. Chen, and E. G. Larsson, "Weighted sum-rate maximization for reconfigurable intelligent surface aided wireless networks," *IEEE Trans. Wireless Commun.*, vol. 19, no. 5, pp. 3064–3076, May 2020.

[10] Z. Yu and D. Yuan, "Resource optimization with interference coupling in multi-RIS-assisted multi-cell systems," *IEEE Open J. Veh. Technol.*, vol. 3, pp. 98–110, 2022.

[11] K. Ying, Z. Gao, S. Lyu, Y. Wu, H. Wang, and M.-S. Alouini, "GMD-based hybrid beamforming for large reconfigurable intelligent surface assisted millimeter-wave massive MIMO," *IEEE Access*, vol. 8, pp. 19530–19539, 2020.

[12] S. H. Hong, J. Park, S.-J. Kim, and J. Choi, "Hybrid beamforming for intelligent reflecting surface aided millimeter wave MIMO systems," *IEEE Trans. Wireless Commun.*, vol. 21, no. 9, pp. 7343–7357, Sep. 2022.

[13] C. Feng, W. Shen, J. An, and L. Hanzo, "Joint hybrid and passive RIS-assisted beamforming for mmWave MIMO systems relying on dynamically configured subarrays," *IEEE Internet Things J.*, vol. 9, no. 15, pp. 13913–13926, Aug. 2022.

[14] R. Li, B. Guo, M. Tao, Y.-F. Liu, and W. Yu, "Joint design of hybrid beamforming and reflection coefficients in RIS-aided mmWave MIMO systems," *IEEE Trans. Commun.*, vol. 70, no. 4, pp. 2404–2416, Apr. 2022.

[15] C. You, Q. Wu, Y. Liu, R. Schober, and A. L. Swindlehurst, "Guest editorial special issue on intelligent reflecting surface for green communication, computing, and sensing," *IEEE Trans. Green Commun. Netw.*, vol. 6, no. 1, pp. 160–162, Mar. 2022.

[16] S. Misra, Y. Gao, N. Gupta, F. Dressler, V. Piuri, and G. Xue, "Guest editorial special issue on energy-efficient reconfigurable wireless communication and networks," *IEEE Trans. Green Commun. Netw.*, vol. 6, no. 2, pp. 665–668, Jun. 2022.

[17] L. You, J. Xiong, D. W. K. Ng, C. Yuen, W. Wang, and X. Gao, "Energy efficiency and spectral efficiency tradeoff in RIS-aided multiuser MIMO uplink transmission," *IEEE Trans. Signal Process.*, vol. 69, pp. 1407–1421, 2021.

[18] C. Huang, A. Zappone, G. C. Alexandropoulos, M. Debbah, and C. Yuen, "Reconfigurable intelligent surfaces for energy efficiency in wireless communication," *IEEE Trans. Wireless Commun.*, vol. 18, no. 8, pp. 4157–4170, Aug. 2019.

[19] L. Du, W. Zhang, J. Ma, and Y. Tang, "Reconfigurable intelligent surfaces for energy efficiency in multicast transmissions," *IEEE Trans. Veh. Technol.*, vol. 70, no. 6, pp. 6266–6271, Jun. 2021.

[20] A. Ihsan, W. Chen, M. Asif, W. U. Khan, Q. Wu, and J. Li, "Energy-efficient IRS-aided NOMA beamforming for 6G wireless communications," *IEEE Trans. Green Commun. Netw.*, vol. 6, no. 4, pp. 1945–1956, Dec. 2022.

[21] Y. Wu, F. Zhou, W. Wu, Q. Wu, R. Q. Hu, and K.-K. Wong, "Multi-objective optimization for spectrum and energy efficiency tradeoff in IRS-assisted CRNs with NOMA," *IEEE Trans. Wireless Commun.*, vol. 21, no. 8, pp. 6627–6642, Aug. 2022.

[22] L. Li, D. Ma, H. Ren, P. Wang, W. Lin, and Z. Han, "Toward energy-efficient multiple IRSs: Federated learning-based configuration optimization," *IEEE Trans. Green Commun. Netw.*, vol. 6, no. 2, pp. 755–765, Jun. 2022.

[23] T. Zhang and S. Mao, "Energy-efficient federated learning with intelligent reflecting surface," *IEEE Trans. Green Commun. Netw.*, vol. 6, no. 2, pp. 845–858, Jun. 2022.

[24] M. Feng, S. Mao, and T. Jiang, "Dynamic base station sleep control and RF chain activation for energy-efficient millimeter-wave cellular systems," *IEEE Trans. Veh. Technol.*, vol. 67, no. 10, pp. 9911–9921, Oct. 2018.

[25] Z. Zheng and H. Gharavi, "Spectral and energy efficiencies of millimeter wave MIMO with configurable hybrid precoding," *IEEE Trans. Veh. Technol.*, vol. 68, no. 6, pp. 5732–5746, Jun. 2019.

[26] M. Sefunç, A. Zappone, and E. A. Jorswieck, "Energy efficiency of mmWave MIMO systems with spatial modulation and hybrid beamforming," *IEEE Trans. Green Commun. Netw.*, vol. 4, no. 1, pp. 95–108, Mar. 2020.

[27] Y. Wang, H. Lu, D. Zhao, Y. Deng, and A. Nallanathan, "Intelligent reflecting surface-assisted mmWave communication with lens antenna array," *IEEE Trans. Cogn. Commun. Netw.*, vol. 8, no. 1, pp. 202–215, Mar. 2022.

[28] Z. Wang, L. Liu, and S. Cui, "Channel estimation for intelligent reflecting surface assisted multiuser communications: Framework, algorithms, and analysis," *IEEE Trans. Wireless Commun.*, vol. 19, no. 10, pp. 6607–6620, Oct. 2020.

[29] J. An, C. Xu, L. Gan, and L. Hanzo, "Low-complexity channel estimation and passive beamforming for RIS-assisted MIMO systems relying on discrete phase shifts," *IEEE Trans. Commun.*, vol. 70, no. 2, pp. 1245–1260, Feb. 2022.

[30] C. Xu et al., "Channel estimation for reconfigurable intelligent surface assisted high-mobility wireless systems," *IEEE Trans. Veh. Technol.*, vol. 72, no. 1, pp. 718–734, Jan. 2023.

[31] Z. Peng et al., "Channel estimation for RIS-aided multi-user mmWave systems with uniform planar arrays," *IEEE Trans. Commun.*, vol. 70, no. 12, pp. 8105–8122, Dec. 2022.

[32] X. Guo, Y. Chen, and Y. Wang, "Wireless beacon enabled hybrid sparse channel estimation for RIS-aided mmWave communications," *IEEE Trans. Commun.*, vol. 71, no. 5, pp. 3144–3160, May 2023.

[33] F. Chapeau-Blondeau and A. Monir, "Numerical evaluation of the lambert W function and application to generation of generalized Gaussian noise with exponent 1/2," *IEEE Trans. Signal Process.*, vol. 50, no. 9, pp. 2160–2165, Sep. 2002.

JITENDRA SINGH (Student Member, IEEE) received the B.Tech. and M.Tech. degrees in electronics and communication engineering with specialization in wireless communication and networks from Gautam Buddha University, Greater Noida, India, in 2017. He is currently working toward the Ph.D. degree with the Department of Electrical Engineering, Indian Institute of Technology Kanpur, Kanpur, India. His research interests include cognitive radio networks, mmWave communication, intelligent reflecting surface, integrated sensing and communication systems. He is a Member of team who won Qualcomm 6G University Research India Program, 2023.

SURAJ SRIVASTAVA (Senior Member, IEEE) received the M.Tech. degree in electronics and communication engineering from the Indian Institute of Technology Roorkee, Roorkee, India, in 2012 and the Ph.D. degree in electrical engineering from the Indian Institute of Technology Kanpur, Kanpur, India, in 2022. From 2012 to 2013, he was employed as a Staff-I Systems Design Engineer with Broadcom Research India Pvt. Ltd., Bengaluru, Indian. From November 2013 to December 2015, he was employed as a Lead Engineer with Samsung Research India, Bengaluru, where he worked on developing layer-2 of the 3G UMTS/WCDMA/HSDPA modem. His research interests include applications of sparse signal processing in 5G wireless systems, mmWave and terahertz communication, orthogonal time-frequency space, joint radar and communication, and optimization and machine learning. He was the recipient of the Outstanding Ph.D. Thesis and Outstanding Teaching Assistant Awards from IIT Kanpur. In 2018 and in 2022, he was awarded Qualcomm Innovation Fellowship (QIF) from Qualcomm.

SURYA P. YADAV (Student Member, IEEE) received the B.Tech. degree in electronics and communication engineering from the Kamla Nehru Institute of Technology, Sultanpur, India, in 2018. He is currently workinf toward the M.Tech. degree in electrical engineering from the Indian Institute of Technology Kanpur, Kanpur, India, specializing in signal processing, communication, and networks. His research interests include physical layer design of 5G wireless systems, cognitive radio system, mmWave communications, and intelligent reflecting surface.

ADITYA K. JAGANNATHAM (Senior Member, IEEE) received the bachelor's degree from the Indian Institute of Technology Bombay, Mumbai, India, and the M.S. and Ph.D. degrees from the University of California at San Diego, San Diego, CA, USA. From 2007 to 2009, he was employed as a Senior Wireless Systems Engineer with Qualcomm Inc., San Diego, where he was a part of the Qualcomm CDMA Technologies Division. He is currently a Professor with the Department of Electrical Engineering, Indian Institute of Technology Kanpur, Kanpur, India, where he also holds the Arun Kumar Chair Professorship. His research interests include next generation wireless cellular and WiFi networks, with a special emphasis on various 5G technologies such as massive MIMO, mmWave MIMO, FBMC, NOMA, and emerging 6G technologies such as OTFS, IRS, THz systems, and VLC. He has been twice awarded the P. K. Kelkar Young Faculty Research Fellowship for excellence in research, received multiple Qualcomm Innovation Fellowships (QIF 2018, 2022). He was the recipient of the IIT Kanpur Excellence in Teaching Award, CAL(IT)2 Fellowship at the University of California at San Diego, Upendra Patel Achievement Award at Qualcomm San Diego, and the Qualcomm 6G UR India gift.

LAJOS HANZO (Life Fellow, IEEE) received Honorary Doctorates from the Technical University of Budapest, Budapest, Hungary, in 2009 and Edinburgh University, Edinburgh, U.K., in 2015. He is a Foreign Member of the Hungarian Science-Academy, Fellow of the Royal Academy of Engineering (FREng), IET, and EURASIP. He was the recipient of the IEEE Eric Sumner Technical Field Award.